Metabolically-Driven Maturation of hiPSC-Cell Derived Heart-on-a-Chip

Nathaniel Huebsch[1†+], Berenice Charrez[1†], Brian Siemons[1], Steven C. Boggess[2], Samuel Wall[3], Verena Charwat[1], Karoline H. Jæger[3], Felipe T. Lee Montiel[1], Nicholas C. Jeffreys[1], Nikhil Deveshwar[1], Andrew Edwards[3], Jonathan Serrano[4], Matija Snuderl[4], Andreas Stahl[5], Aslak Tveito[3], Evan W. Miller[2,6], Kevin E. Healy[1,7*]

1. Department of Bioengineering and California Institute for Quantitative Biosciences (QB3), University of California at Berkeley, Berkeley, California 94720, USA

2. Department of Chemistry, University of California at Berkeley, Berkeley, California 94720, USA

3. Simula Research Laboratory, 1325 Lysaker, Norway

4 Department of Pathology, New York University Langone Health and Medical School, New York, NY, 10016, USA

5 Department of Nutritional Sciences and Toxicology, University of California at Berkeley, Berkeley, California 94720, USA

6 Department of Molecular and Cell Biology, University of California at Berkeley, Berkeley, California, 94720, USA

7 Department of Materials Science and Engineering, University of California at Berkeley, Berkeley, California, 94720, USA

† These authors contributed equally to this work

+ Current Affiliation: Department of Biomedical Engineering, The Washington University in Saint Louis, Saint Louis, Missouri, 63130, USA

* Corresponding author: Kevin E. Healy, PhD, 370 Hearst Memorial Mining Building, # 1760, Berkeley, CA 94720

Telephone: (510) 643-3559

Email: kehealy@berkeley.edu

Running Title: Metabolically Driven Maturation of hiPSC-Derived Heart-On-A-Chip

Keywords: Microphysiological Systems, Induced Pluripotent Stem Cells, Tissue Chips

Abstract

Human induced pluripotent stem cell derived cardiomyocytes (hiPSC-CM) are a promising *in vitro* tool for drug development and disease modeling, but their immature electrophysiology limits their diagnostic utility. Tissue engineering approaches involving aligned and 3D culture enhance hiPSC-CM maturation but are insufficient to induce electrophysiological maturation. We hypothesized that recapitulating post-natal switching of the heart's primary adenosine triphosphate source from glycolysis to fatty acid oxidation could enhance maturation of hiPSC-CM. We combined hiPSC-CM with microfabrication to create 3D cardiac microphysiological systems (MPS) that enhanced immediate microtissue alignment and tissue specific extracellular matrix production. Using Robust Experimental design, we identified a maturation media that allowed the cardiac MPS to correctly assess false positive and negative drug response. Finally, we employed mathematical modeling and gene expression data to explain the observed changes in electrophysiology and pharmacology of MPS exposed to maturation media. In contrast, the same media had no effects on 2D hiPSC-CM monolayers. These results suggest that systematic combination of biophysical stimuli and metabolic cues can enhance the electrophysiological maturation of hiPSC-derived cardiomyocytes.

Introduction

Human induced pluripotent stem cell (hiPSC) technology provides an exciting opportunity to model human disease in the laboratory. hiPSC-derived cardiomyocytes (hiPSC-CM) are especially promising in terms of their ability to model heart tissue and have great potential as biological tools for drug development, gene editing, and treating biological and environmental threats. An immediate goal for cardiac tissue models is to reduce and refine the use of animal testing in the drug development pipeline. Inherent differences between species have historically diminished the ability of animal models to prognosticate drug safety and efficacy. Microphysiological systems (MPS), or organ-chips, combine 3D-architecture of tissue micro-environments with the ability to interrogate key physiological functions (for example, cardiomyocyte action potential) and well-defined delivery profiles for nutrients.

A challenge with using hiPSC-CM to predict drug safety and efficacy is the immaturity of hiPSC-CM (Ogle *et al.* 2016, Vunjak Novakovic *et al.* 2014, Robertson *et al.* 2013). In particular, hiPSC-CM exhibit automaticity (spontaneous beating without electrical stimulation) and longer action potentials (415±22msec for ventricular-like hiPSC-CM, versus 270-300msec directly measured by patch-clamp of primary human adult left-ventricular cardiomyocytes (Iseoka et al. 2018, Lemoine et al. 2017, Paci *et al.* 2015, Ma *et al.* 2011). Culturing hiPSC-CM or human embryonic stem cell (hESC) derived cardiomyocytes (hESC-CM) within the *in vivo*-like microenvironment of Engineered Heart Muscle (EHM; Shadrin et al. 2017, Huebsch et al. 2016, Mannhardt, *et al.* 2016, Godier-Furnemont *et al.* 2015, Hinson et al. 2015, Zhang et al. 2013, Nunes et al. 2013, Tulloch et al. 2011, Tiburcy et al. 2011, Zimmermann et al. 2002), or MPS (Mathur et al. 2015) has been shown to mature hiPSC-CM to some extent, enhancing physiologic hypertrophy, and leading to pharmacology more closely correlated to the one of the adult human heart.

In addition to 3D culture approaches, bioreactor-based strategies such as chronic electrical pacing or cyclic strain (typically applied over 2-4 weeks in culture), have been shown to enhance maturity of hESC-CM and hiPSC-CM (Ronaldson-Bouchard *et al.* 2018; Ruan *et al.* 2015, Godier-Furnemont *et al.* 2015, Nunes *et. al* 2013). Collectively these methods are promising, but no single approach applied thus far has been sufficient to induce full maturation of pluripotent stem cell derived cardiomyocytes. Furthermore, many of the existing approaches require prolonged culture periods (in some cases approaching one

month), large scale formats, and/or complex setups to execute. These issues would lead to cost and logistical limitations to their translation to higher-throughput analyses that would be essential to use these technologies for applications like drug development.

As bioreactor approaches have limited scalability, and tissue engineered microenvironments alone are not sufficient to induce hiPSC-CM maturation consistent with the adult heart, there has been a focus on combining tissue engineering approaches with soluble cues. Transplanting hiPSC-CM into neonatal rodent hearts enhances maturation (Kadota et al. 2017), suggesting that the soluble milieu of the heart is compatible with this process. Reductionist approaches have used specific soluble cues from the fetal and post-natal heart, including cytokines (Rupert et al. 2017, Tiburcy *et al.* 2017), micro-RNAs (Kuppusamy et al. 2015), heart specific extracellular matrix (Fong *et al.* 2016) and hormones (Yang *et al.* 2014) to enhance the maturity of hESC-CM and hiPSC-CM.

The metabolic milieu is a key component of cells' soluble environment. Postnatally, the heart switches from glycolysis to fatty-acid oxidation as its primary source of Adenosine triphosphate (ATP; Lopaschuck *et al.* 2010, Makinde *et al.* 1998). Previously, 2D hiPSC-CM monolayers and engineered tissues exposed to glucose-depleted, fatty-acid enriched media exhibited more mature metabolic profiles and physiology compared to hiPSC-CM cultured in standard media (Correira *et al.* 2018, Mills *et al.* 2017, Rana et al. 2012). However, fatty-acid based media has not been studied in the context of MPS. We hypothesized that the combination of aligned, 3D culture and fatty-acid could enhance electrophysiological maturation of hiPSC-CM within cardiac MPS. Using a Design of Experiments approach, (Jha *et al.* 2014, Stile et al. 2002, Phadke et al. 1989), we identified fatty-acid based Maturation Media (MM) that induced a shortened, adult-like Action Potential Duration (APD), and enhanced the pharmacologic relevance of hiPSC-based MPS. MM-treated MPS also exhibited changes in expression of ion-channel and calcium handling genes, including Sarcolipin (SLN). In contrast, the same media had no effects on 2D hiPSC-CM monolayers. Combined with mathematical modeling, gene expression changes in MM-cultured MPS explained a significant amount of the observed changes in action potential and pharmacology.

Results and Discussion

Robust Design Experiments Indicate Optimal Carbon Sourcing for Mature Beating Physiology

We have developed a microfabricated cardiac MPS, employing hiPSC-CM, for drug testing (Mathur et al. 2015). In the present study, we formed cardiac MPS that that mimicked the mass composition of the human heart by combining 80% hiPSC-CM and 20% hiPSC-SC (**Supplemental Methods, Fig. S1-2**). We employed Robust Experimental Design to screen for the effects of glucose, oleic acid, palmitic acid, and albumin (bovine serum albumin, BSA) levels on hiPSC-CM maturity (**Table 1**). MPS were incubated with different fatty-acid media for ten days, at which time their beating physiology and calcium flux were assessed. Optimal media would reduce automaticity (e.g. reduce spontaneous beating rate), while also reducing the interval between peak contraction and peak relaxation (a surrogate for APD) in field-paced tissues (**Fig. 1A-C**), while maintaining a high level of beating prevalence during pacing (defined as the percent of the tissue with substantial contractile motion; **Fig. 1D**). In general, beating prevalence was consistent with calcium flux amplitude (**Fig. 1D,F**), and beating interval correlated with rate-corrected Full-Width Half Maximum calcium flux time, FWHMc; **Fig. 1B,E**).

These screening experiments suggested a less significant role for oleic and palmitic acid in inducing shortened beating intervals and calcium transient duration (**Fig. 1B,E**). However, a closer examination of the data revealed that, although complete glucose deprivation in MPS treated with media having only oleic acid or palmitic acid eliminated beating, treatment with glucose-free media that was supplemented with both fatty acids (Media 9; **Fig. 1H**) partially rescued this deficiency. This is consistent with the ability of hiPSC-CM to use both these fatty acids as ATP sources. Thus, we concluded that the optimal media should include both palmitic and oleic acids. Furthermore, although absolute glucose deprivation would likely force fatty acid oxidation, the severe effects of complete glucose deprivation on beating prevalence and calcium flux prompted us to adjust the glucose level in idealized media to a low, non-zero level of 0.5g/L (2.75mM), about 10% of the level in standard B-27 supplemented RPMI Media used to culture hiPSC-CM, and add 10mM of galactose. Previous work has established galactose combined with fatty acids as a viable ATP source for healthy iPSC-cardiomyocytes in monolayer cultures (Rana *et al.* 2012, Wang *et al.* 2014).

As the inclusion of higher levels of BSA appeared to diminish beating interval without severely affecting prevalence or calcium flux, we concluded that an ideal maturation media would contain this higher level (2.5%, vs. 0.25% contained in standard, B-27 supplemented media). This lead to a new Maturation Media (herein referred to as “MM”), comprised of glucose free RPMI basal media supplemented with 2% B-27, 0.5g/L glucose (2.8mM), 10mM galactose, 2.25% BSA (to a final concentration of 2.5% BSA including albumin contained in B-27), 200μM oleic acid and 100μM palmitic acid. MM exhibited a substantial portion of the beneficial effects of glucose free, fatty acid enriched media on reducing beating interval, without suffering as severe a loss of beating prevalence (**Fig. 1H, I**).

Maturation-Media Induced Changes in Action Potential, but only for Cardiac MPS

MM reduced APD from the prolonged levels we observed for Standard Media (RPMI containing B-27 supplement, herein referred to as “SM”) treated MPS (**Fig. 2A**). Interestingly, however, switching from SM to MM had no measurable effects on APD or automaticity when hiPSC-CM were cultured in confluent 2D monolayers (**Fig. 2C**). Due to potential concerns about cytotoxicity of high levels of BSA and palmitic acid (Naim et al. 1995, Park et al. 2014), we also repeated APD studies on MPS treated with MM in which we independently varied levels of these two components. The complete absence of BSA and palmitic acid from MM led to APD that was not significantly different from APD observed for SM treated MPS (M1;

Fig. 2E). In the absence of palmitic acid, the addition of a high dose of BSA appeared to be somewhat toxic to cardiac tissues, as the prevalence of beating in these samples (M2) was nearly zero, making it difficult to interpret the apparent APD in those tissues (**Fig. 2F**). Interestingly, palmitic-acid enriched media still had significant effects on APD reduction, while negative effects of high albumin dosing were slightly reduced, when the total amount of albumin present was reduced below 2.5%. However, since the APD observed with 0.25% BSA (M3; **Fig. 2E**) was significantly lower than the APD for adult human left ventricular cardiomyocytes, we assumed these tissues might fall outside the ideal physiologic range for drug testing. Thus, MM with 200µM oleic acid, 100µM palmitic acid, 0.5g/l glucose, 10mM galactose and 2.5% BSA was used for all subsequent studies.

Although several types of fatty acids have been shown to enhance maturation of hiPSC-CM monolayers and engineered heart tissues, here we found that it was necessary to include palmitic acid specifically (**Fig. 2E**). This suggests that although generalized metabolic effects such as oxidation-induced DNA damage response (Mills et al. 2017) is likely important to electrophysiological maturation of hiPSC-CM *in vitro*, events affected directly by palmitic acid, such as palmitoylation of calcium channel subunits (Bodi et al. 2005) or receptors (Liu et al. 2012) may also be involved. Furthermore, although it was possible to reduce APD with maturation media that included oleic acid and palmitic acid without increased albumin (**Fig. 2E**), this treatment yielded APD that fell below the target range of adult cardiomyocytes. It is possible that albumin, which is a fatty-acid carrier *in vivo*, provided a more temporally-stable dose of fatty acids to cells cultured within the MPS. The concentration of albumin in MM is not markedly dissimilar from the 3.5-5% albumin level found in human blood. Finally, the finding that fatty-acid based maturation media had significant effects on action potential and pharmacology within MPS, but not 2D hiPSC-CM monolayers, suggests the need to incorporate advanced 3D culture models during development of protocols to mature hiPSC-CM, and likely other hiPSC-derived tissue cells.

Pre-Treatment of hiPSC-Derived-Cardiomyocyte Based MPS with Maturation Media Supports Inotropic Responsiveness

MM treatment did not result in changes in gross sarcomere structure within MPS, as assessed by staining for sarcomeric α-Actinin (ACTN2; **Fig. 3A**). Quantitative analysis of sarcomere morphology with Fourier-Transform based methods (Wang *et al.* 2014, Ma *et al.* 2018) was consistent with these qualitative observations, and suggested no substantial changes in sarcomere organization as a result of MM treatment (**Fig. 3B**). When we directly measured force developed in MPS via the deflection of PDMS pillars in the chamber (**Supplemental Methods; Fig. S3)**, we found that both SM and MM-pre-treated MPS exhibited a robust dose response to increased extracellular calcium, with a maximal range of stress similar to adult human heart tissue slices (**Fig. 3C**; data on adult slices calculated from Brandenburger et al. 2011). Consistent with work by Mills, we observed that fatty-acid based maturation media neither inhibited nor enhanced peak twitch force (Mills *et al.* 2017). However, MM pre-treated MPS were sensitized to lower concentrations of extracellular calcium than SM pre-treated controls, with a statistically significant EC_{50} of 0.11±0.06 mM for MM pre-treated MPS versus 0.95±0.46mM for SM-pre-treated controls ($p < 0.05$, 2-way *t*-test). Furthermore, MM pre-treated MPS showed a statistically significant steeper fold-increase in force in response to extracellular calcium over the linear region of the calcium-force response curve, with an initial slope of 12±1.5 $mN/mm^2/mM\ Ca^{2+}$ versus 3.9±0.26 for SM-pre-treated controls ($p < 0.01$, 2-way *t*-test). MM pre-treated MPS showed a trend toward desensitization to isoproterenol, and a lower peak force induced by this drug, when compared to SM pre-treated MPS. However, these differences were not statistically significant (**Fig. 3D**). Similarly to inotropic effects of

isoproterenol assessed at constant (paced at 1Hz) beat-rate, MM pre-treatment appeared to slightly desensitize MPS to the chronotropic effects of isoproterenol, although, as with inotropic effects, the changes were not statistically significant (**Fig. 3E**). The EC50 values for isoproterenol chronotropy fell within the range recently reported for engineered heart tissue subjected to exercise-induced maturation via external pacing (Ronaldson-Bouchard *et al.* 2018).

EC_{50} values changed depending on the parameter analyzed, and hence cannot be quantitatively compared to each other. Even though EC50 values in SM treated MPS are in the same range for both inotropy and chronotropy measurements, MM treated MPS show higher EC_{50} values for inotropy data compared to chronotropy analysis. Collectively, these data suggested that MM does not damage sarcomeres or interfere with excitation-contraction coupling or adrenergic responsiveness and enhances calcium contraction coupling when the amount of extracellular calcium is limiting.

Pre-Treatment of hiPSC-Derived-Cardiomyocyte Based MPS with Maturation Media Enhances Prediction of Drug Induced ProArrhythmia

We next assessed whether maturation media treatment could lead to more predictive pharmacology on compounds with known effects on QT interval. When we analyzed Verapamil dose-escalation effects in field-paced MPS and used beating prevalence as the metric for characterizing IC_{50}, we observed that MM-pre-treated MPS exhibited enhanced Verapamil resistance compared to SM-treated MPS (971 nM for MM-pre-treated MPS, versus 90nM for SM-treated MPS; **Fig. 4A**). Direct analysis of APD revealed a dose-dependent decrease in APD_{90} as a function of increasing Verapamil dose, consistent with the clinical application of this drug to shorten QT duration (**Fig. 4B,C**). However, unlike beating prevalence, the dose-response for normalized APD_{90} did not change appreciably in MM pre-treated, compared to SM-pre-treated MPS. This suggests that the observed prevalence changes may depend on calcium dynamics or other processes downstream of the action potential.

Flecainide, a class Ic (Na+ channel blocker) antiarrhythmic drug typically used to treat tachy-arrythmia, has been noted to have a narrow therapeutic index and is counter-indicated in patients with pre-existing structural disease (Aliot *et al.* 2011). Consistent with this narrow therapeutic index, we correctly observed very little difference between the IC_{50} for this drug and the Estimated Therapeutic Plasma Concentration (ETPC) of 1.5µM, when either beating prevalence or APD_{90} were used as metrics of toxicity (**Fig. 4D-F**). Unlike Verapamil, Flecainide did not exhibit a differential IC_{50} within MM versus standard media pre-treated MPS.

Finally, we assessed beating IC_{50} of Alfuzosin, an α_1-adrenergic blocking agent that has been shown to increase patients' QT interval by hERG-independent mechanisms (Lacerda *et al.* 2008, Lian *et al.* 2013). Here, we observed that both MM and SM pretreated MPS exhibited IC_{50} near 1µM when measuring beating prevalence (**Fig. 4G**). However, when we tested the effects of this drug on extending APD_{90}, we observed a specific sensitization with MM-pre-treated MPS, relative to MPS cultured in SM (**Fig. 4H-I,K**).

We summarized these observations of drug responsiveness by plotting the safety ratio observed for each drug, using either beating prevalence (**Fig. 4J**) or APD_{90} prolongation (**Fig. 4K**) as the metric used to determine IC_{50}. The safety margin is defined as *in vitro* IC_{50}/ETPC, and describes the relative risk for beating abnormalities. None of these drugs exhibited differential pharmacology between SM and MM-pre-treated 2D monolayers (data not shown). This revealed that both MPS and the subsequent maturation of MPS with fatty-acid enriched media had effects on the safety margin for Verapamil (using the metric of prevalence) and Alfuzosin (using the metric of APD_{90}), but no statistically significant effect

on the safety margin of Flecainide (**Fig. 4J,K**). There was also a trend, albeit not statistically significant, toward sensitization (lower safety margin) of beating prevalence to Alfuzosin in both SM and MM pre-treated MPS, compared to 2D monolayers. These data suggest that MPS improves the prognostic capability of hiPSC-CM, and that MM pre-treatment further augments the prognostic power of MPS. For example, although Verapamil is routinely used in the clinic, particularly for QT-interval management, it exhibits false positive toxicity in hERG-assays, and the beating prevalence of 2D monolayer cultures of hiPSC-CM are sensitized to this drug, as shown here (**Fig. 4J**) and in other studies (Mathur et al. 2015, Huebsch et al. 2016, Liang et al. 2013). Our data suggests that culture within MPS alone dramatically enhances the IC_{50} of this drug, eliminating the false positive toxicity seen in 2D monolayer hiPSC-CM culture consistent with our previous study (Mathur *et al.* 2015 and **Fig. 4J**). The combination of MPS with MM gives a more accurate profile of the safe nature (thereby reducing false positive toxicity) of this drug. In contrast, the fact that Alfuzosin is sometimes observed to cause arrhythmias in the clinic (Lacerda *et al.* 2008), suggests that the higher *in vitro* IC_{50} values observed in monolayer culture and SM-cultured MPS under-predict potential toxicity (false negative). Our findings with MM-cultured MPS, which indicate sensitization to the APD prolongation effects of Alfuzosin, suggest that MM pre-treatment enhances the ability of MPS to accurately predict the clinically observed effects of this drug.

Altogether, these data indicate that combining MPS culture with MM can reduce both false positive (Verapamil) and false negative (Alfuzosin) drug response estimates. Enhanced drug resistance is not universally observed in MPS culture, suggesting against the trivial explanation that drug availability is limiting in these 3D systems, likely due to the small and physiologically-relevant scale of our 3D microtissues ~ 150um in width, consistent with cardiac muscle bounded by collagen fibrils (Kanzaki *et al.* 2010). This suggests instead that changes in drug susceptibility are due to changes in density and function of specific ion channels that these drugs target.

Gene Expression Changes caused by Maturation Media in MPS-Cultured hiPSC-Derived Cardiomyocytes

Direct analysis of gene expression in SM versus MM treated hiPSC-CM monolayers indicated no significant difference in expression of a panel of ion channels and sarcomere related genes. Consistent with observations regarding the immaturity of hiPSC-CM, several ion channel transcripts were either deficient or overexpressed in these cells, when compared to commercially available RNA obtained from adult human hearts (**Fig. 5A**). This includes HCN4, a gene partially responsible for the “funny current” I_f that maintains automaticity in adult nodal cells and immature ventricular cardiomyocytes. Further, the absolute level of SCN5A and several other ion channel transcripts, including KCNJ2, was highly variable between different batches of purified, 2D monolayer hiPSC-CM. This may point to mis-regulation of expression in these channels in non-physiologic culture formats, or to differences in the relative composition of different cardiomyocyte populations obtained from our small molecule-based differentiation protocol (Lee *et al.* 2017).

We next directly assessed gene expression in RNA obtained from MPS treated for ten days with either SM or MM. Interestingly, and in contrast to results by Mills *et al.* (Mills *et al.* 2017), we did not observe significant variation in expression of the glycolysis associated gene, GAPDH, relative to other potential “housekeeping” genes (data not shown). Analysis of a panel of genes involved in electrophysiology, cell identity, contractility and calcium handling did not reveal a global shift in expression as would be expected for gross changes in cell differentiation or population composition (**Fig. 5B**). Further, we did not observe substantial differences in the expression of most potassium channels including hERG (KCNH2).

However, KCND2 was shown to be downregulated with MM (**Fig. 5C**). The genes most significantly upregulated by MM were SLN, HCN2 and CACNB2 (**Fig. 5B,C**). Sarcolipin (SLN) normally suppresses the SERCA pump, thereby suppressing calcium flux from the cytosol to the sarcoplasmic reticulum (Gorski *et al.* 2017). The β-subunit of the voltage activated calcium channel expression, CACNB2, is required for expression of the *L*-type calcium current through regulating trafficking and activation of α-subunits (Bodi *et al.* 2005, Venetucci *et al.* 2012). Despite our observation that force production and inotropic responsiveness of MPS were not perturbed by MM pre-treatment, we observed substantial downregulation of several genes associated with calcium handling and sarcomere function, including MYL2/MLC2V, and MYH7, as well as increased expression of SLN (**Fig. 5B,C**).

Mathematical modeling of the ion channel and calcium transient contribution to electrophysiological patterns in pre-treated MPS and monolayer

Newly developed mathematical models (Tveito *et al.* 2018) were applied to estimate the contribution of individual Na^+, K^+, and Ca^{2+} channels, along with calcium handling machinery, to the action potential and calcium transients of hiPSC-CM monolayers and SM or MM treated MPS (**Fig. 6A-C**). Consistent with gene expression data, simulations predicted no change in the total conductance ($g_x \bullet C_m \bullet A/V$) for two major potassium currents, I_{K1} and I_{Kr} (hERG) (**Fig. 6D**). There was a trend toward reduction in Na^+ current in MM versus SM treated MPS ($p < 0.05$, 2-way *t*-test), although globally, there was no significant difference observed amongst the different culture conditions ($p = 0.08$, ANOVA) (**Fig. 6E**).

Simulations suggested a marked effect of MM treatment on the sodium-calcium exchange current in MPS, with a highly significant, nearly 4-fold reduction (**Fig. 6F**). There were no predicted changes in the magnitude of either RYR2 receptor activity or *L*-type calcium flux (**Fig. 6G,H**) as a function of media type, although MM treatment appeared to significantly increase the magnitude of *L*-type calcium current in 2D monolayer versus MPS. Interestingly, although MM-induced treatment promoted massive upregulation of SLN (**Fig. 5**), which interacts with and suppresses the activity of the SERCA pump, there was no significant change in SERCA pump activity suggested by these simulations (**Fig. 6I**). This may reflect the post-transcriptional regulation of SLN activity (e.g. phosphorylation; Gorski *et al.* 2017). In contrast, the simulated intracellular calcium diffusion rate, which accounts for other sources of intracellular transport, including binding to the sarcomeres, was markedly upregulated in MM-treated MPS compared to other conditions (**Fig. 6J**). This increased intracellular Ca^{2+} transport would be consistent with enhanced sarcomere activation at low availability of calcium, due to depleted extracellular calcium or blocked *L*-type calcium channels, and is thus consistent with our observation of enhanced force development in MM versus SM treated MPS at low levels of extracellular calcium (**Fig. 4C**), and the relatively high IC_{50} value for contractile motion (without a concurrent shift in IC_{50} for APD) in MM versus SM treated MPS (**Fig 5A-C**). Finally, consistent with gross observations of overall cell shape provided by sarcomere analysis (**Fig. 4**), simulations predicted no significant change in cellular surface to volume ratio (**Fig. 6K**).

While our optimization strategy did not involve kinetic parameters for any transporters, the highly non-linear relationship among the various transporters and membrane voltage can cause changes in the current time courses that may not be expected from changes in their conductance parameters. To provide a mechanistic explanation of how the various changes to conductance resulted in pronounced AP shortening for MM treated MPS, we calculated the net charge transported by the major inward and outward current carriers over various intervals of the simulated APs (**Fig. 7A**). Consistent with the lower simulated I_{NaCa} for MM treated MPS, the integrated flux through this transporter indicated reduced total

inward current compared to all other conditions (**Fig. 7B**). In the model this effect occurs over the time frame of 100-200 msec following peak action potential, and is also due in part to a more rapid transport of calcium from the membrane to the intracellular compartment where it interacts with the myofilaments. In this time-frame inward I_{NaCa} and I_{CaL} combine to slow repolarization driven by progressive recruitment of the delayed rectifier currents (I_{Ks} and I_{Kr}), and thus a reduction in I_{NaCa} allows the repolarizing currents to predominate more rapidly. Consistent with the observation of similar *L*-type Ca^{2+} flux, there was no change in the integrated I_{CaL} over this time-frame (**Fig. 7C**), and thus the overall flux of calcium was dominated by I_{NaCa}. This also resulted in reduced integrated calcium source current for MM-treated MPS compared to SM-treated MPS or 2D monolayers (data not shown). As shown in **Fig. 6D**, both I_{K1} and I_{Kr} activated significantly more rapidly in MM-treated MPS compared to the other conditions (**Fig. 7D,E**), however because both of these currents only conduct at negative potentials, this was entirely driven by the altered time course of repolarization rather than any differences in simulated transporter expression.

Although maturation-media induced a striking upregulation of SLN, this was not strongly linked to the shortening of APD in our system. Normally, SLN, like Phospholamban, acts to inhibit the SERCA pump, yet data from our simulations obtained by fitting our action potential and calcium transient data to the modified Paci model of hiPSC-CM electrophysiology (Paci *et al.* 2015) suggested that any contribution of SR calcium reuptake to AP shortening is not consistent with the simultaneous calcium and AP time courses (**Fig. 6**). This is to be expected as reduced SERCA flux would tend to force calcium to be extruded via forward-mode I_{NaCa} which in turn prolongs the AP. It is possible that SLN may be turned on at a transcriptional level, while transcriptional levels of the contractility genes MYL2 and MYH7 are reduced, in response to changes in cellular metabolic milieu and biophysical cues experienced with MM in MPS. The downregulation of sarcomere genes and the lack of MM-enhancement of baseline force (at physiological levels of extracellular Ca^{2+}) or inotropy in MPS suggest that further soluble cues, such as hormones and/or cytokines (Parikh *et al.* 2017, Yang *et al.* 2014), along with chronic electrical pacing (Richardson-Bouchard et al. 2018) may be required to complete hiPSC-CM maturation.

Conclusions

Despite the promise of hiPSC-derived tissue cells as genetically defined human *in vitro* models for drug development and fundamental biology, maturation of hiPSC derivatives including hiPSC-CM into adult-like cells remains an important challenge. In the present study, we demonstrated that the combination of aligned, 3D culture in MPS with fatty-acid based media synergized to promote maturation of hiPSC-CM action potential. Combining *in silico* modeling with experimental measurements provided insights into a putative mechanism linking alterations in individual ion channels and calcium handling machinery to whole-cell changes in action potential. This was the first study to induce maturation of hiPSC-CM in a tissue-chip, and, importantly, we demonstrated that maturation not only affected the baseline physiology of hiPSC-CM, but also yielded cells with pharmacology more reminiscent of adult human cardiomyocytes. These results suggest that maturation with fatty-acid based media may be a prerequisite to using hiPSC-CM based tissue chips to predict how drugs will affect the adult human heart.

Experimental Procedures

Cell Sourcing

All studies were performed with Wild Type C (WTC) human hiPSC harboring a single-copy of CAG-driven GCaMP6f knocked into the first Exon of the AAVS1 "safe harbor" locus (Huebsch *et al.* 2015). The parent cell line (WTC) was reprogrammed from fibroblasts derived from a healthy 30-year-old Japanese adult male with a normal electrocardiogram and no known family history of heart disease and is available from the Coriell Repository (# GM25256 hiPSC from Fibroblast).

Cardiomyocyte Differentiation

hiPSC-CM were derived from pluripotent WTC and purified using published protocols relying on small molecular manipulation of Wnt signaling (Lian *et al.* 2012, Ma *et al.* 2014), with some modifications. Briefly, frozen stocks of pluripotent cells were thawed and plated on hESC-Qualified Matrix (Corning; Corning, NY) in Essential 8 Medium (E8; Thermo Fisher, Tewksbury, MA) containing 10μM Y27632 (Peprotech; Rocky Hill, NJ). Fresh E8 without drug was added the following day. To prepare cells for differentiation, hiPSC were grown to 70-80% confluency, and then passaged three times at a constant density of 20,000 cells/cm^2 (Burridge *et al.* 2014). During passaging, cells were singularized with Accutase (Thermo; Waltham, MA) and plated in E8 with 10μM Y27632. After pre-passaging, hiPSC were plated at a density of 25,000 cells/cm^2, in 10μM Y2762. This was counted as "day – 3" of differentiation. At day 0, hiPSC were >90% confluent and were treated with Roswell Park Memorial Institute Medium 1640 (RPMI) containing B-27 supplement without insulin (RPMI-I), along with 8μM CHIR99021 (Peprotech) and 150μg/mL *L*-ascorbic acid (LAA). Exactly 24 hr after drug was added, medium was exchanged for RPMI-I (day 1). On day 2, medium was replaced with RPMI-I containing 5μM IWP-2 (Peprotech). On day 4, medium was exchanged for RPMI-I. RPMI containing standard B-27 supplement (RPMI-C) was added on days 6,7, 9, and 11. Robust spontaneous contractile activity was typically observed on day 8 of differentiation.

On day 15 of differentiation, hiPSC-CM were singularized and cryopreserved. Prior to this, cells were washed twice, for 15 minutes, with dPBS, to deplete calcium from extracellular space and sarcomeres. Next, cells were exposed to 0.25% Trypsin (Thermo, Waltham, MA) for 10-20 minutes. Cells were triturated gently at every five minutes, then pelleted (300g, 5 minutes). Cell pellets were resuspended into RPMI-C with 10μM Y27632 for counting. Cells were then pelleted a second time, and resuspended into cryopreservation medium containing 10μM Y27632, then frozen and kept in liquid nitrogen.

Two weeks before MPS experiments, hiPSC-CM were thawed and plated at a density of 100,000 cells/cm^2 onto Matrigel, in RPMI-C with 10μM Y27632. The following day, medium was exchanged for RPMI-C. Three days after plating, monolayers were spontaneously contracting. Cells were then washed with dPBS and exposed to a cardiomyocyte selective medium depleted of glucose and pyruvate (Media-L; RPMI 1640 without glucose or sodium pyruvate, supplemented with 23mM sodium bicarbonate and 5mM Sodium *L*-lacate; Toyhama *et al*. 2013) for a total of five days. Cells were washed with dPBS and fresh Media-L was added every other day. On the fifth day of purification, significant death of non-beating cells was observed. Cells were washed with dPBS and allowed to recover in RPMI-C for three days. Cardiomyocyte purity both before and after this procedure was characterized by flow cytometry for Cardiac Troponin T (TNNT2; **Fig. S1**).

Isogenic Stromal Cell Differentiation

Isogenic iPS-stromal cells (hiPSC-SC) were derived via small molecular activation of Wnt signaling in pluripotent hiPSC, followed by VEGF exposure, as described previously (Lian et al. 2014). Briefly, hiPSC were seeded at a density of 25,000 cells/cm^2 onto hESC-Qualified Matrigel. This was termed “day -3” of the culture. On day 0, wells were 80-100% confluent, and the medium was switched to LaSR media (Advanced F12/DMEM, 2.5mM Glutamax; 60ug/ml ascorbic acid), and 7.5uM CHIR99021 for 2 days without medium change. At day 2, the media was changed to LSR media with 50 ng/ml VEGF (Peprotech) for 2 days without medium change. On day 4, medium was replaced to LaSR media only. On day 6, cells were ready for CD31 magnetic sorting. For magnetic sorting on day 6 of differentiation, cells were rinsed with dPBS and trypsinized for 8min. Trypsin was quenched by adding EB20 media (20% FBS, 2.5mM Glutamax, KO DMEM), and cells were centrifuged (300g for 3 minutes) and re-suspended in FACS buffer (PBS, 2% FBS). CD31+ magnetic Dynabeads were added to the cell suspension at a concentration of 8 beads per CD31+ cell and left 20min on ice. The CD31 negative fraction was then expanded (maximum of ten passages) on uncoated tissue culture plastic substrates supplemented with EGM-2 media (Lonza) and characterized (**Fig. S2**).

Plating of hiPSC-CM for 2D Monolayer Studies

In 2D monolayers, hiPS-SC overgrow hiPS-CM (data not shown). Thus, for 2D pharmacology and gene expression studies, biochemically purified hiPSC-CM were grown in monolayers. Purified cardiomyocytes were singularized with 0.25% trypsin after extensive dPBS washes. The cells were then resuspended into RPMI-C supplemented with 10μM Y27632 and plated at a density of 200,000 cells/cm^2 onto GFR Matrigel. The following day, medium was exchanged for RPMI-C. Three days after plating, monolayers were spontaneously contracting. Cells were then exposed to either SM or MM for ten days prior to the onset of gene expression and pharmacology studies.

Fabrication of Cardiac MPS

Microfluidic cardiac MPS systems were formed using small modifications of the protocol described in our previous work (Mathur *et al.* 2015; see Fig. S3). Briefly, two-step photolithography was used to form a chip comprised of 1) a cell-loading port leading to a cell culture chamber with two large “anchoring posts” and several smaller micro-posts and 2) a media-loading port leading to media channels running alongside the cell culture chamber. The media channels and cell culture chamber (50μm high) are connected by a series of fenestrations (2μm high) that provide a mechanical barrier to convective flow, such that all media factors delivered to cells in the culture chamber arrive via diffusion (Mathur *et al.* 2015). The cardiac MPS is formed by molding Polydimethylsiloxane (PDMS; Sylgard 184 kit, Dow Chemical, Midland, MI) at a 10:1 ratio of Sylgard base to crosslinker. These PDMS chambers were then bonded to glass slides using oxygen plasma.

Self-Assembly of Cardiac Microtissues within Cardiac MPS

hiPSC-CM and hiPSC-SC (passage 5 - 8) were singularized with 0.25% trypsin after extensive PBS washes. We then prepared a cocktail of 80% hiPSC-CM and 20% hiPSC-SC, at a density of 6.6x10^6 cells/mL, in EB20 media supplemented with 10μM Y27632 and 150μg/mL *L*-ascorbic acid. 3μL of this cocktail, corresponding to 2x10^4 cells, was injected into the cell loading inlet of each MPS. MPS were then loaded by centrifugation (300g, 3 minutes), and plugged with an SP20 steel rod to prevent cellular regurgitation from the cell chamber during media loading. Next, the same media used to resuspend cells

was added to the channels of each MPS. MPS were then individually inspected, and any cell chambers that were not completely filled were filled by applying gentle pressure to the SP20 plug. This time-point was counted as MPS day 0. At MPS day 1, media was changed to RPMI with B27 supplement. At day 3 MPS were continuously fed either maturation media or standard media, using negative pressure for media exchange as described in our previous study (Mathur *et al.* 2015). Media was changed every 2-3 days.

Robust Design Experiments to identify the composition of the optimal maturation media

We hypothesized that switching the carbon source of cardiac MPS from glucose to fatty acids could induce more mature electrophysiology of hiPSC-CM. We employed Robust Design screening to optimize four different media composition variables. Given the likelihood of these variables acting in a synergistic fashion to enhance maturation, the parametric space would require 3^4, or 81 independent experiments (excluding the several replicates required for significant studies) To study this large space in a cost and time-effective manner within MPS, we employed Robust Design screening. With orthogonal arrays, the variable-space spanned by these 81 independent experimental conditions was explored with only 9 independent experiments. These 9 experiments were designed such that the four media input variables (levels of glucose, oleic acid, palmitic acid and BSA) were varied in an orthonormal fashion from one experiment to the next (**Table 1**). In the case where glucose was completely omitted from cardiac media, we added 10mM galactose, as previous studies have shown healthy hiPSC-CM are capable of using galactose as an ATP source (Wang et al. 2014). Based on the hydrophobic nature of the primary fatty acids used as ATP sources in the heart (oleic acid and palmitic acid, respectively), we added additional BSA, above the 0.25% already contained in the B27 supplement. Beating physiology and calcium flux were assessed with high-speed microscopy as described below. Media were screened based on their ability to reduce spontaneous beat-rate, as well as the interval between peak contraction and peak relaxation during 1Hz field pacing, while maintaining a high prevalence of beating (defined as the percent of the tissue with time-averaged motion exceeding a pre-determined threshold) during pacing at 1Hz. MPS were treated with various candidate maturation media for 10 days before beating physiology was assessed.

Image Acquisition for Beating Physiology Studies

During imaging, MPS or 2D monolayers in multi-well plates were maintained at 37°C on a stage equipped with a heating unit (Tokai Hit, Gendoji-cho, Japan). First, baseline readings of spontaneous calcium flux (GCaMP6), and beating physiology (bright-field video) were taken. After acquiring spontaneous electrical activity, electromechanical activity under field pacing was assessed. MPS were paced via sterile, blunted stainless steel needles that were inserted into the pipette tips leading to both the media inlets and outlets. Care was taken to fill pipettes and prevent bubble formation to maintain electrical conductivity. Before recording videos, cells were paced for 10 seconds (20V, 20msec bipolar pulses at 1Hz, ION OPTIX Myopacer Field Simulator). Pacing was then maintained at the same intensity and frequency for acquiring images of MPS contracting at 1Hz.

Imaging was performed with a NIKON TE300HEM microscope equipped with a HAMAMATSU digital CMOS camera C11440 / ORCA-Flash 4.0. All videos were recorded at a framerate of 100 frames/second for a duration of 8 seconds. For GCaMP imaging, fluorescent excitation was provided by a Lumencor SpectraX Light Engine (GCaMP: Cyan LED, 470nm) and filtered with a QUAD filter (Semrock). Videos were acquired using Zeiss Zen Pro 2012 software.

Image Analysis

Brightfield videos were analyzed for beating physiology using an updated version of our open source motion tracking software (Huebsch *et al. Tissue Eng. C.* 2015; software available at https://huebschlab.wustl.edu/resources/). The current version of the software uses tools from the open source Bioformats Toolbox (Linkert *et al.* 2010) to obtain image and metadata from microscopy files.

Briefly, microscopy files (Zeiss Zen, .czi) were directly read into the Matlab-based GUI, and the contractile motion of tissues was analyzed via an exhaustive-search block-matching optical flow algorithm that compared the position of 8x8 pixel macroblocks at frame *i* to their position at frame *i*+5 (corresponding to the motion in 50msec). Motion vectors were used to calculate beat-rate, beating interval (defined as the time delay between maximum contraction velocity and maximum relaxation velocity, which is directly proportional to action potential duration), and beating prevalence. Beating prevalence was defined as the percentage of macroblocks within a region-of-interest (ROI) with a time-averaged contraction speed that exceeds a defined threshold (2μm/sec was defined empirically as a universal threshold for all MPS analyzed). ROI were selected to include the entire cell culture chamber of the MPS.

GCaMP data were quantified using in-house Matlab code that was developed based on previous work by Laughner and colleagues (Laughner *et al.* 2012; Ma *et al.* 2018). GCaMP videos were analyzed for τ_{75} decay time (time for calcium amplitude to go from maximum to 25% of maximum), as well as peak intensity, a metric of total calcium influx. For spontaneously beating cells, data on beating interval and calcium transient decay times were rate corrected using Fridericia's method (Fridericia 1920).

Optical Measurement of Action Potentials

BeRST-1 dye was synthesized, and purity verified, as previously described (Huang et al. 2015). For action potential recording, MPS were first labeled overnight with 2.5μM BeRST-1. The following day, MPS were equilibrated to media without dye before imaging (RPMI-C without phenol red) as described above, using a Red LED (640nm). For monolayer experiments, cells were labeled with 500nM BeRST-1 for 1h at 37°C, and then equilibrated to RPMI-C without phenol red. After acquiring videos of spontaneous and 1Hz paced activity at 100 Hz for 8 seconds, BeRST-1 videos were analyzed using similar Matlab code as was used for GCaMP analysis (Laughner *et al.* 2012). BeRST-1 videos were analyzed for 90% Action Potential Duration (APD_{90}). Reported values of APD_{90} (**Fig. 2**) are for MPS or monolayers paced at 1Hz.

Measurement of contraction force

Micro-molded polydimethylsiloxane (PDMS) pillars were added to the cell chambers, so that the tissue would deflect them upon each contraction (**Fig. S3**). By considering each pillar as a cantilever beam fixed at one end and uniformly loaded with horizontal forces along its height, one can apply the Euler-Bernouilli formula for uniformly distributed load and deduce the contraction force from the pillar's elastic modulus, deflection and dimensions. Pillar deflection was calculated with ImageJ by measuring the distance between the pillar's centroid coordinates before and after contraction. Same scale (0.5 pixel/micron) was used for all measurements.

Pharmacology in MPS and 2D Monolayers

To avoid any possible confounding effects that different albumin or lipid content might have on drug bioavailability, for all pharmacology, MPS were first equilibrated to phenol red free RPMI with B-27 (SM)

containing vehicle control (DMSO, methanol, or water, to a final concentration of 0.1% v/v). On the day upon which studies were performed, freshly measured drug was dissolved into DMSO, except for Flecainide, which came as a methanol stock solution, and Verapamil, which was dissolved directly into media. For testing inotropic responsiveness to extracellular calcium concentration and isoproterenol, Tyrode's saline (0.1g/L anhydrous $MgCl_2$, 0.2g/L KCl, 8g/L NaCl, 50mg/L anhydrous monobasic sodium phosphase, 1g/L D-glucose) was used in lieu of RPMI-C, as in previous studies of inotropic responsiveness of macroscale and miniaturized EHM (Huebsch et al. 2016, Zhang *et al.* 2013). After recording activity in zero-dose vehicle condition, media were exchanged for the lowest drug dose, and MPS were incubated for 30 minutes at 37°C. Spontaneous activity, and activity with 1 Hz pacing, were recorded as described above. This was repeated for each dose escalation of drug. Drug dose was escalated until all spontaneous and paced activity ceased, or a dose of 10μM was reached.

Media on monolayers of hiPSC-CM was replaced with phenol red free RPMI-C containing 1μM BeRST-1, and monolayers were incubated for 30 minutes at 37°C (5% CO_2). Medium was next replaced with RPMI-C supplemented with the vehicle used to dissolve drug (water, methanol or DMSO, to a final concentration of no more than 0.1% v/v). Similar to dose-escalation studies in MPS, new drug was added and allowed to equilibrate to each increasing drug dose over 30 minutes intervals at 37°C, 5% CO_2. After equilibrating monolayers to vehicle and to each dose of drug, spontaneous beating physiology, calcium flux and action potentials were collected in bright-field, GCaMP and BeRST-1 channels, respectively. Next, cells were paced at 1Hz to collect these same three parameters.

Gene Expression in Monolayer Culture

To characterize gene expression during hiPSC-SC differentiation, cells at various stages of differentiation of hiPSC to endothelial cells were trypsinized, pelleted and lysed (Qiagen RLT lysis buffer supplemented with 1% β-Mercaptoethanol. RNA was recovered using spin columns (Qiagen MicroRNAeasy® kit), with on-column DNAse I digest performed according to the manufacturer's protocol. Purified hiPSC-CM were plated to a density of 200,000 cells/cm^2 on Matrigel coated plates in RPMI-C containing 10μM Y27632. One day after plating medium was exchanged for RPMI-C. Two days following this, monolayers had recovered spontaneous beating, and cells were treated for ten days with either Standard Media (SM) or Maturation Media (MM). Media was exchanged every 3 days. On day 10, cells were washed with PBS and RNA was recovered in the same manner as for monolayer hiPSC-SC. Following RNA recovery from 2D cultures, 500ng of recovered RNA was used to produce cDNA using the SuperScript III kit with Oligo-dT primers (Life Technologies). The obtained cDNA was used to perform SYBR Green and Taqman real-time PCR analysis with the probes described in Supplemental Tables S1 and S2. Commercial polyA-RNA obtained from 15 pooled male/female Caucasians adult human left ventricle (Clonetech, Mountain View, CA) was used as a positive control for expression of cardiomyocyte ion channels, as described previously by Liang *et al.* (Liang *et al. Circulation* 2013).

Gene Expression in MPS

Purified hiPSC-CM were combined with expanded hiPSC-SC as described above for initial optimization studies and cultured for ten days in either standard SM or MM. We first optimized protocols for isolating high-quality (R.I.N. > 8.5) RNA from MPS (data not shown). RNA was extracted from tissue using methods similar to those previously applied for macroscale engineered heart muscle preparations (Mannhardt et al. 2016, Nunes et al. 2013). Briefly, on day 10, MPS were flushed for 10 minutes with PBS at 25°C. Following this wash, MPS were carefully cut with a sterile scalpel, to separate the cell culture chamber from the cell loading chamber of the MPS, and to open the device. The PDMS

component, with microtissue attached, was transferred to a microcentrifuge tube, and pooled with up to six other microtissues in lysis buffer from the RNAqueous kit (Thermo). Immediately after adding the tissues to lysis buffer, the microcentrifuge tube containing them was flash frozen in liquid nitrogen. Next, RNA was retrieved from samples by following manufacturer instructions on the RNAqueous kit, followed by DNAse I digestion (Ambion). The yield and quality of RNA were assessed with Qbit and Bioanalyzer, and with optimized methods, we routinely achieved RNA Integrity Numbers above 9. RNA isolated from MPS was amplified using a SMARTeR stranded Pico Input Total RNA library prep kit (Clonetech). The cDNA library products were then diluted by a factor of 10 into sterile water for direct quantitative PCR analysis of relative gene expression. RNA from positive controls was reverse-transcribed and amplified using the same kit. For qPCR analysis, cDNA libraries were diluted by a factor of ten into RNA grade water so that gene expression would fall within the linear assay range.

MPS Tissue Isolation and Immunofluorescence Imaging

Tissues were treated with SM or MM for 10 days. On day 10, MPS were flushed for 10 minutes with PBS at 25°C. Following this wash, 4% PFA was added to the media channel for 15min to fix the tissues. MPS were washed with PBS twice for 5min after that and were then carefully cut with a clean scalpel, to open the device and expose the tissue. At this point, the PDMS component had the tissue structure attached to it. The tissues were then stained by submerging PDMS blocks in different staining solutions: First, tissues were blocked with blocking buffer (1% BSA 10% FBS 0.5% Triton 0.05% sodium azide) overnight at 4˚C. The next day, they were submerged in 1:1000 DAPI solution (Invitrogen D1306) in blocking buffer for 30-40 minutes at 25˚C. Tissues were then treated with the primary antibodies (Mouse anti α-actinin, Life technologies 41811) 1:100 concentration in blocking buffer) for 48h at 4˚C. Tissues were then washed twice at 25˚C in blocking buffer for 2-3 hours and washed a third time at 4˚C overnight. The secondary antibody (Goat anti-mouse IgG Alexa 568 H+L, Life Technology a11004) was added overnight at 4˚C at a 1:100 concentration in blocking buffer. Tissues were then washed twice at 25˚C in blocking buffer for 2-3 hours and a third time at 4˚C overnight before tissues were imaged.

Imaging was performed with an Olympus BX51W1 upright microscope equipped with Prairie Techologies Aurora SFC lasers and Quantum 512SC camera. All images were taken through an Olympus LUMPlan FL 60x water immersion lens (N.A. 1.00, FN 26.5). Images were acquired using Prairie View 5.3 U3 Beta software. We imaged both DAPI and α-actinin for sarcomere alignment using 405nm and 546nm lasers respectively. The settings were the following: binning 1x1, Aperture 35um slit, emission quad.
We performed z-stacks over 2μm with a step-size of 0.25μm with 128x averaging for each image. Post imaging processing was performed on ImageJ to enhance contrast and decrease background fluorescence.

To analyze the regularity of sarcomeres from staining of sarcomeric α-Actinin, we applied Fast Fourier-Transform (FFT) based methods (Ma *et al.* 2018) to cellular regions of the MPS that had a constant size (100 x 100 pixels). Next, the real component of the FFT was smoothed with a 3x3 Gaussian filter, and the mean intensity was calculated as a function of radial distance from the center of the centered real-component of the FFT. Structures with regularly repeating features (e.g. sarcomeres) produce distinct bands when analyzed in this manner, resulting in local increases in intensity at specific radial distance. These local intensity increases were quantified (Ma *et al.* 2018, Wang *et al.* 2014). Code is available from the authors upon request.

Mathematical Modeling

Time-series of AP and Ca^{2+} flux from MPS paced at 1Hz were inverted to a mathematical model of ion channel activity and calcium dynamics to obtain simulated estimates of channel conductance and calcium handling as described in our recent publication (Tveito *et al.* 2018). Briefly, a modified version of a model of an immature stem cell (Paci *et al.* 2015) was used to calculate the predicted voltage and calcium dynamics. Parameters of this model, specifically maximal channel conductances, intracellular calcium diffusion terms, and surface to area ratios, were then iteratively perturbed until the error between the measured waveforms and simulated waveforms was minimized. Resulting parameters and produced action potential models were then plotted by group to provide an explanation for mechanistic reasons for changes in action potential.

Statistical Analysis

Direct comparisons were made by non-paired student's *t*-test, with Holm-Bonferonni correction for multiple comparisons. All curve fitting was done using GraphPad Prism. IC_{50} and EC_{50} curves were fit to four-parameter models. When these models yielded ambiguous fits (Fig. 4A, 5C, 5D, 5F and 5G), a three-parameter model was used. Gene expression data were statistically analyzed with ClustVis (web tool for clustering multivariate data) and GraphPad Prism. Overall PCR data were plotted on ClustVis to obtain heatmaps of the gene expression for maturation media treated MPS relative to standard media values. The genes within 70% percentile of differential expression were then selected and plotted on GraphPad Prism where a t-test was performed to compare standard media and maturation media values using the Holm-Sidak method. Significance was determined with p-value < 0.05.

Acknowledgements

This work was funded in part by the California Institute for Regenerative Medicine DISC2-10090 (K.E.H.), NIH- NIH-NHLBI HL130417 (K.E.H.), the Research Council of Norway INTPART Project 249885, the SUURPh program funded by the Norwegian Ministry of Education and Research,and the Peder Sather Center for Advanced Study (UC Berkeley). We thank Mary West (UC Berkeley) for assistance with image analysis and flow cytometry and Silvio Weber (Technische Universität Dresden) and Stacey Renschler (Washington University in St. Louis) for helpful advice on RNA isolation, cDNA amplification and data analysis. We thank Yoram Rudy, Jon Silva and Jianmin Cui (Washington University in St. Louis) for critical discussion on action potential acquisition, mathematical modeling and data analysis.

Professor Kevin E. Healy has a financial relationship with Organos Inc. and both he and the company may benefit from commercialization of the results of this research.

References

Artman, M., Graham, T., Boucek, R. (1985). Effects of postnatal maturation on myocardial contractile response to calcium agonists and changes in contraction frequency. *J. Cardivascular Pharmacol*., vol. 7, no. 5, pp. 850–855, 1985.

Aliot, E., Capucci, A., Crijins, H.J., Goette, A., Tamargo, J. (2011). Twenty-five years in the making: flecainide is safe and effective for the management of atrial fibrillation. *EP Eurospace*; 13(2): 161-73.

Birket, M.J., *et al.* (2015). Contractile Defect Caused by Mutation in MYBPC3 Revealed Under Conditions Optimized for PSC-Cardiomyocyte Function. *Cell Rep.* 13(4): 733-45.

Bodi, I., Mikala, G., Koch, S.E., Akhter, S.A., Schwartz, A. (2005) The L-type calcium channel in the heart: the beat goes on. *J. Clin. Invest.* 115(12): 3306-17.

Brandenburger, M., *et al.* (2011). Organotypic slice culture from human adult-ventricular myocardium. *Cardiovasc Res.* 93(1): 50-9.

Burridge, P.W., *et al.* (2014). Chemically defined generation of human cardiomyocytes. *Nat Methods.* 11(8): 855-60.

Correia, C., *et al.* (2017). Distinct carbon sources affect structural and functional maturation of cardiomyocytes derived from human pluripotent stem cells. *Sci. Rep*; 7(1): 8590.

Correia C., *et al.* (2018). 3D aggregate culture improves metabolic maturation of human pluripotent stem cell derived cardiomyocytes. *Biotechnol. Bioeng.* 11593): 630-44.

Crandall, S.H. (1978). *An Introduction to the Mechanics of Solids,* ed. Lardner, T.J. (McGraw-Hill, New York), 511-576.

Fong, A.H., *et al.* (2016). Three-Dimensional Adult Cardiac Extracellular Matrix Promotes Maturation of Human Induced Pluripotent Stem Cell-Derived Cardiomyocytes. T*issue Eng Part A.* 22(15-16): 1016-25.

Fridericia, L.S. (1920). The duration of systole in the electrocardiogram of normal subjects and of patients with heart disease. *Acta Medica Scadinavica* 53: 469-86.

Godier-Furnemont, A.F.G., *et al.* (2015). Physiologic force-frequency response in engineered heart muscle by electromechanical stimulation. *Biomaterials* 60: 82-91.

Gorski, P.A., Ceholski, D.K., Young, H.S. (2017). Structure-Function Relationship of the SERCA Pump and Its Regulation by Phospholamban and Sarcolipin. *Adv Exp Med Biol.* 981: 77-119.

Hinson JT, *et al* (2015). HEART DISEASE. Titin mutations in iPS cells define sarcomere insufficiency as a cause of dilated cardiomyopathy. *Science* 349(6251): 982-6.

Huang, Y.L., Walker, A.S., Miller, E.W. (2015). A Photostable Silicon Rhodamine Platform for Optical Voltage Sensing. *J. Am. Chem. Soc.* 137: 10767-76.

Huebsch, N., Loskill, P., *et al.* (2015). Automated video-based analysis of contractility and calcium flux in human-induced pluripotent stem-derived cardiomyocytes cultured over different spatial scales. *Tissue Eng. Part C. Methods*. 21(5): 467-79.

Huebsch, N., *et al.* (2016). Miniaturized iPS-Cell-Derived Cardiac Muscles for Physiologically Relevant Drug Response Analysis. *Sci. Rep.* 6: 24726.

Iseoka, H. et al. (2018). Pivotal Role of Non-cardiomyocytes in Electromechanical and Therapeutic Potential of Induced Pluripotent Stem Cell-Derived Engineered Cardiac Tissue. *Tissue Eng.* Part A 24, 287–300.

Jha, A.K., Jackson, W.M., Healy, K.E. (2014). Controlling osteogenic stem cell differentiation via soft bioinspired hydrogels. *PLOS One.* 9(6): e98640.

Kadota S, Pabon L, Reinecke H, Murry CE. (2017). In Vivo Maturation of Human Induced Pluripotent Stem Cell-Derived Cardiomyocytes in Neonatal and Adult Rat Hearts. *Stem Cell. Rep.* 8(2): 278-89.

Kanzaki, Y., et al. (2010). Three-dimensional architecture of cardiomyocytes and connective tissue in human heart revealed by scanning electron microscopy. *Criculation* 122: 1973-4.

Kuppusamy, K. et al. (2015). Let-7 family of microRNA is required for maturation and adult-like metabolism in stem cell-derived cardiomyocytes. *PNAS*. 201424042

Lacerda, A.E. et al. (2008). Alfuzosin Delays Cardiac Repolarization by a Novel Mechanism. *Journal of Pharmacology and Experimental Therapeutics*. 324 (2) 427-433

Laughner, J.I., et al. (2012). Processing and analysis of cardiac optical mapping data obtained with potentiometric dyes. *Am. J. Physiol. Heart Circ. Physiol*. 303: H753-65.

Lee, J.H., et al. (2017). Human Pluripotent Stem Cell-Derived Atrial and Ventricular Cardiomyocytes Develop from Distinct Mesoderm Populations. *Cell Stem Cell*. 21(2): 179-94.

Lemoine, M. D. et al. (2017). Human hiPSC-derived cardiomyocytes cultured in 3D engineered heart tissue show physiological upstroke velocity and sodium current density. *Sci. Rep*. 7, 5464.

Lian, X., *et al.* (2012). Robust cardiomyocyte differentiation from human pluripotent stem cells via temporal modulation of canonical Wnt signaling. *Proc. Natl. Acad. Sci. USA.* 109(27): E1848-57.

Lian, X., *et al.* (2014). Efficient differentiation of human pluripotent stem cells to endothelial progenitors via small-molecule activation of WNT signaling. *Cell Reports.* 3(5): 804-16.

Liang P, *et al.* (2013). Drug Screening Using a Library of Human Induced Pluripotent Stem Cell-Derived Cardiomyocytes Reveals Disease-Specific Patterns of Cardiotoxicity.

Linkert, M., *et al.* (2010). Metadata matters: Access to image data in the real world. *J Cell Biol.* 189:777-82.

Liu, R., Wang, D., Shi, Q., Fu, Q., Hizon, S., Xiang, Y.K. (2012). Palmitoylation regulates intracellular trafficking of β2 adrenergic receptor/arrestin/phosphodiesterase 4D complexes in cardiomyocytes. *PLOS One*. 7(8): e42658.

Lopaschuck, G. et al. (2010), Energy Metabolic Phenotype of the Cardiomyocyte During Development, Differentiation, and Postnatal Maturation. *Journal of Cardiovascular Pharmacology*. 56:130-140.

Ma, J., et al. (2011). High purity human-induced pluripotent stem cell-derived cardiomyocytes: electrophysiological properties of action potentials and ionic currents. *Am J Physiol. Heart Circ. Physiol* 301: H2006-17.

Ma, Z., *et al.* (2014). Three-dimensional filamentous human diseased cardiac tissue model. *Biomaterials* **35**:1367-1377.

Ma, Z., Huebsch, N., Koo, S., *et al.* (2018). Synergy of MYBPC3 Deficiency and Mechanical Overload Leads to Contractile Deficits in Engineered Cardiac Tissue. *Nat. Biomed. Eng.* In Press.

Makinde, AO. et al. (1998). Maturation of fatty acid and carbohydrate metabolism in the newborn heart. *Molecular and Cellular Effects of Nutrition on Disease Processes. Developments in Molecular and Cellular Biochemistry*, vol 26. Springer, Boston, MA

Mannhardt I, *et al.* (2016). Human Engineered Heart Tissue: Analysis of Contractile Force. *Stem Cell Reports* 7: 29-42.

Mathur, A., *et al.* (2015). Human hiPSC-based cardiac microphysiological system for drug screening applications. *Sci. Rep.* 5:8883.

McDevitt, T.C., Laflamme, M.A., Murry, C.E. (2005). Proliferation of cardiomyocytes derived from human embryonic stem cells is mediated via the IGF/PI3-kinase/Akt signaling pathway. *J. Mol. Cell. Cardiol.* 39: 865-73.

Mills, R.J., *et al.* (2017). Functional screening in human cardiac organoids reveals a metabolic mechanism for cardiomyocyte cell cycle arrest. *Proc. Natl. Acad. Sci. USA.* 114(40: E8372-81.

Minamisawa, S., *et al.* (2003). Atrial Chamber-specific Expression of Sarcolipin is Regulated during Development and Hypertrophic Remodeling. *J Biol. Chem.* 278(11): 9570-5.

Murry, C.E., Keller, G. (2008). Differentiation of Embyronic Stem Cells to Clinically Relevant Populations: Lessons from Embryonic Development. *Cell.* 132(4): 661-80.

Navarrete, E.G., *et al.* (2013). Screening drug-induced arrhythmia [corrected] using human induced pluripotent stem cell-derived cardiomyocytes and low-impedance microelectrode arrays. *Circulation* 129(15): e452.

Nguyen, D.C., *et al.* (2014). Microscale generation of cardiospheres promotes robust enrichment of cardiomyocytes derived from human pluripotent stem cells. *Stem Cell Reports.* 3(2): 260-8.

Naim, J. et al. (1995). The effect of molecular weight and gel preparation on humoral, adjuvancy of silicone oils and silicone gels. *Immunological investigation*. 24:537-547

Nunes SS, *et al.* (2013). Biowire: a platform for maturation of human pluripotent stem cell-derived cardiomyocytes. *Nat Methods* 10(8): 781-7.

Ogle, B.M., *et al.* (2016). Distilling complexity to advance cardiac tissue engineering. *Sci. Transl. Med.* 8(342): 342ps13.

Paci, M., Hyttinen, J., Rodriguez, B., Severi, S. (2015). Human induced pluripotent stem cell-derived versus adult cardiomyocytes: an in silico electrophysiological study on effects of ionic current block. *Br. J. Pharmacol.* 172(21): 5147-60.

Parikh, S.S., *et al.* (2017). Thyroid and Glucocorticoid Hormones Promote Functional T-tubule Development in Human-Induced Pluripotent Stem Cell Derived Cardiomyocytes. *Circ. Res.* 121(12): 1323-30.

Park, E.J, et al. (2014). Multiple pathways are involved in palmitic acid-induced toxicity. *Food and Chemical Toxicology*. 67:38-34

Phadke, S. M., (1989). Quality Engineering Using Robust Design, Prentice Hall, Englewood Cliffs, N.J.

Rana, P., Anson, B., Engle, S., Will, Y. (2012). Characterization of Human-Induced Pluripotent Stem Cell-Derived Cardiomyocytes: Bioenergetics and Utilization in Safety Screening. *Toxicol Sci.* 130(1): 117-31.

Ribeiro, M.C., *et al.* (2015). Functional maturation of human pluripotent stem cell derived cardiomyocytes in vitro—corelation between contraction force and electrophysiology. *Biomaterials* 51: 138-50.

Robertson, C., Tran, D.D., George, S.C. (2013). Concise review: maturation phases of human pluripotent stem cell-derived cardiomyocytes. *Stem Cells.* 31(5): 829-37.

Ronaldson-Bouchard, K., *et al.* (2018). Advanced maturation of human cardiac tissue grown from pluripotent stem cells. *Nature*. 556: 239-43.

Ruan JL, *et al.* (2015). Mechanical Stress Promotes Maturation of Human Myocardium from Pluripotent Stem Cell-Derived Progenitors. *Stem Cells*. 33(7): 2148-57.

Rupert CE, Coulombe KLK (2017). IGF1 and NRG1 Enhance Proliferation, Metabolic Maturity, and the Force-Frequency Response in hESC-derived Engineered Cardiac Tissues. *Stem Cells International* Article ID: 7648409.

Shadrin, I.Y,, *et al.* (2017). Cardiopatch platform enables maturation and scale-up of human pluripotent stem-cell derived engineered heart tissues. *Nat. Commun.* 8(1): 1825.

Stile, R.A., *et al.* (2002). Sequential robust design methodology and X-ray photoelectron spectroscopy to analyze the grafting of hyaluronic acid to glass substrates. *J Biomed Mater Res.* 61(3): 391-8.

Stoehr A., *et al.* (2014). Automated analysis of contractile force and Ca^{2+} transients in engineered heart tissue. *Am J Physiol Heart Circ Physiol.* 306: H1353-63.

Thavandiran, N., *et al.* (2013). Design and formulation of functional pluripotent stem cell-derived cardiac microtissues. *Proc. Natl. Acad. Sci. USA.* 110(49): E4698-707.

Tiburcy, M., *et al.* (2011). Terminal differentiation, advanced organotypic maturation, and modeling of hypertrophic growth in engineered heart tissue. *Circ Res* 109: 1105-1114.

Tiburcy, M., Zimmermann, W.H. (2014). Modeling myocardial growth and hypertrophy in engineered heart muscle. *Trends Cardiovasc Med.* 24(1): 7-13.

Tiburcy, M., *et al.* (2017). Defined Engineered Human Myocardium with Advanced Maturation for Applications in Heart Failure Modeling and Repair. *Circulation* 135(19): 1832-47.

Toyhama, S., *et al.* (2013). Distinct metabolic flow enables large-scale purification of mouse and human pluripotent stem cell-derived cardiomyocytes. *Cell Stem Cell.* 12(1): 127-37.

Tulloch, N.L., *et al.* (2011). Growth of engineered human myocardium with mechanical loading and vascular coculture. *Circ Res.* 109(1): 47-59.

Tveito, A., Jaeger, K.H., Huebsch, N., Charrez, B., Edwards, A.G., Wall, S., Healy, K.E. (2018). Inversion and computational maturation of drug response using human stem cell derived cardiomyocytes in microphysiological systems. In Press. *Sci. Rep.*

Venetucci, L., Denegri, M., Napolitano, C., Priori, S.G. (2012) Inherited calcium channelopathies in the pathophysiology of arrhythmias. *Nat. Rev. Cardiol.* 9(10). 561-75.

Vunjak Novakovic, G., Eschenhagen, T., Mummery, C. (2014). Myocardial tissue engineering: in vitro models. Cold Spring Harb Perspect Med. 4(3): pii: a014076.

Wang, G., McCain, M.L., *et al.* (2014). Modeling the mitochondrial cardiomyopathy of Barth syndrome with induced pluripotent stem cell and heart-on-a-chip technologies. *Nat Med.* 20(6): 616-23.

Yang, X. et al (2014). Tri-iodo-l-thyronine promotes the maturation of human cardiomyocytes-derived from induced pluripotent stem cells. *Journal of Molecular and Cellular Cardiology*. 72:296-304.

Zhang, D., et al. (2013). Tissue-engineered cardiac patch for advanced functional maturation of human ESC-derived cardiomyocytes. *Biomaterials*. 34: 5813-20.

Zhang, H., Bradley, A. (1996). Mice deficient for BMP2 are nonviable and have defects in amnion/chorion and cardiac development. *Development* 122(10): 2977-86.

Zimmermann, W.-H. et al. (2002). Tissue engineered of a differentiated cardiac muscle construct. *Circ Research*. 2002;90:223-230

Table 1. Design of Experiments (L9) for Media Screening

Media Formulation	Glucose Concentration (mM)	Oleic Acid Concentration (μM)	Palmitic Acid Concentration (μM)	Bovine Serum Albumin Concentration (mg/mL)
1* (Standard Media, SM)	25	0	0	2.5++
2	25	100	100	10
3	25	200	200	25
4	10	100	0	25
5	10	200	100	2.5
6	10	0	200	10
7&	0	200	0	10
8&	0	0	100	25
9&	0	100	200	2.5
10& (Maturation Media, MM)	2.75	200	100	25
M1&	2.75	200	0	2.5
M2&	2.75	200	0	25
M3&	2.75	200	100	2.5
M4&	2.75	200	100	10

***** The composition of Media 1 is identical to standard RPMI used to feed hiPSC-CM. All media were prepared from the same batch of powdered, glucose free RPMI.

++ The B-27 supplement contains 2.5mg/mL BSA; thus, in media formulations containing only 2.5mg/mL BSA, no extra albumin was added to the system.

& Medias without glucose, and MM, were supplemented with 10mM galactose

In addition to the ingredients described above, all media were supplemented with 2% B-27 supplement and 150μg/mL *L*-ascorbic acid.

Figure Legends

Figure 1. Design-of-Experiments (DoE) Based Screens Identify Maturation Media for hiPSC-CM Microphysiological Systems. A) Approach used for initial screen. Computational motion capture is performed on bright-field videos of contracting cardiac MPS. These videos are used to analyze the prevalence of beating (center; percent of the tissue that moves with average speed above a defined threshold that is held constant for all tissues) and the contraction time (right; defined as the distance between peaks in motion speed for contraction and relaxation, which approximates the interval over which displacement occurs). The knock-in reporter, GCaMP6f, is used to monitor the timing (rate corrected Full-Width-Half-Maximum, FHWMc) and amplitude of calcium transients in MPS. **B-F)** Results from representative L9 Taguchi Array experiments, depicting **B)** beating interval, **C)** spontaneous beating frequency, and **D)** tissue beating prevalence, all obtained from motion tracking analysis, along with calcium transient **E)** FWHMc and **F)** amplitude, obtained from analysis of GCaMP6f fluorescence. **G)** Summary L9 analysis. 1-way ANOVA tests were performed to assess the effects of specific media components, and increases in the parameters measured were denoted as * or ** for *p*-values of 0.05 and 0.01, respectively. **H-I)** Comparison of MPS cultured in standard media (red) to MPS cultured in glucose-free media during L9 studies (black), and MPS cultured in the final Maturation Media (blue). MPS were examined for the effects of glucose depletion and fatty acid addition on **H)** beating prevalence and I) beating interval. Note, beating prevalence and calcium amplitude are ideally maximized, while beating interval, spontaneous beat rate, and calcium transient FWHMc, are ideally minimized, in adult left ventricular cardiomyocytes. MPS were cultured for ten days prior to analysis for the L9 experiments. Data: **B-F**: plot of mean ± SEM, $n = 9$; **H-I**: all data points with median, $n = 3\text{-}12$, except for beating interval in media 8, which could only be calculated in one sample (no other samples cultured in this media exhibited either spontaneous or paced beating) ** $p < 0.01$, * $p < 0.05$ (2-way *t*-test with Holm-Bonferonni correction for multiple comparisons).

Figure 2. Action Potential Characterization of Matured Cardiac MPS. A-C) Representative voltage tracings for **A,B)** MPS and **C)** 2D monolayers cultured for one week in either (**A**) standard cardiac media, or (**B**) Maturation Media (MM). Voltage tracings were obtained by overnight labeling of MPS or monolayers with BeRST-1. **D)** Quantitative analysis of 90% action potential duration (APD_{90}) for MPS (closed shapes) and monolayers (open shapes), cultured in standard cardiac media (SM; red) or maturation media (blue). MM-pretreated MPS had significantly reduced APD_{90} compared to MPS cultured in SM, or either 2D culture. In contrast, the difference in APD_{90} between MPS cultured in SM and cardiomyocytes cultured in 2D was not significant. **E-F)** Analysis of changes in (**E**) APD_{90} and (**F**) contractile prevalence in MM-pretreated MPS that resulted from modulating the levels of palmitate and albumin in MM. Removing both palmitate and albumin from MM (M1) resulted in MPS with APD_{90} that were significantly higher than APD_{90} of MM-treated MPS, and which were no different from APD_{90} of SM-treated MPS. Removal of Palmitate alone (M2), or of albumin alone (M3) led to a new medium that exhibited APD_{90} significantly less than MM ($p < 0.05$). Compared to MM, M2 treated MPS exhibited slightly reduced beating prevalence, whereas this metric was enhanced for M3 treated MPS, although these changes were not statistically significant. Slight reduction of the albumin content of MM from 2.5% to 1% (M4) did not have significant effects on APD_{90} or prevalence of motion in MPS, compared to those treated with MM. All data: plot of all points with median, $n > 5$. (** $p < 0.01$, 2-way *t*-test with Holm-Bonferonni correction for multiple comparisons).

Figure 3. Inotropic Responsive of Maturation Media Treated MPS. A) Representative confocal micrographs depicting sarcomere morphology (Sarcomeric α-Actinin Staining, green, with DAPI nuclear counterstain, blue) of MPS treated for ten days with either standard media (SM) or maturation media

(MM). **B)** Quantification of sarcomeric order in MPS treated with SM versus MM. **C)** Maximum contractile stress generated by MPS pre-treated with either SM or MM as a function of extracellular calcium (delivered in Tyrode's saline). The translucent green box denotes the force generated by adult human heart slice cultures (reference: Brandenburger *et al.* 2011). **D-E)** Normalized (**D**) force and (**E**) beat-rate as a function of isoproterenol dose in SM and MM pre-treated MPS. For force calculation (inotropy), MPS were cultured in Tyrodde's saline with 0.9mM Ca^{2+}. For beat rate calculation (chronotropy), MPS were cultured in Standard Media. Data: mean ± *SEM*, *n* = 3-5. Scale bars: **A**: left panels, 20μm and right panels, 10μm.

Figure 4. Proarrhythmia Pharmacology of Matured Cardiac MPS. IC_{50} analysis was performed in MPS pretreated for ten days with either Maturation Media (blue curves) or Standard Media (Red Curves). For all studies, MPS were equilibrated to Standard Media, and then exposed to escalating doses of **A-C)** Verapamil, **D-F)** Flecainide, and **G-I)** Alfuzosin. IC_{50} curves were obtained by measuring beating prevalence (**A,D,G**) or 90% Action Potential Duration (APD_{90}; **C,F,I**). Representative, intensity normalized action potential traces are depicted for MM-pretreated MPS for each drug (**B,E,H**). Estimated Therapeutic Plasma Concentration (ETPC) values were obtained from the literature. **J-K)** Safety margins (the ratio of *in vitro* IC_{50} to literature values for ETPC) calculated based on **J**) beating prevalence and **K**) APD_{90}. All MPS were paced at 1 Hz for pharmacology analysis. Data: mean ± *SEM*, *n* = 3-5. (* $p < 0.05$, 2-way *t*-test with Holm-Bonferroni correction for multiple comparisons).

Figure 5. Gene Expression analysis of Monolayers and MPS Treated with Lipid-Based Maturation Media. A) Quantitative RT-PCR analysis of expression of ion channel and sarcomere transcripts in hiPSC-CM 2D monolayers after ten days of culture in either Standard (SM; red) or Maturation Media (MM; blue). None of the genes tested exhibited statistically significant expression changes as a result of Maturation Media. Data: plot of points with median, *n* = 4. **B)** Heat-map of relative gene expression in MM-treated MPS as compared to SM-treated MPS, as assessed by qRT-PCR on cDNA libraries amplified from RNA isolated of MPS treated for ten days with SM or MM. **C)** Specific analysis, indicating individual biological replicates (treatments of hiPSC-CM obtained from independent differentiations) of differentially expressed transcripts for ion channels or sarcomere genes in MM and SM treated MPS. MPS PCR data were plotted on ClustVis (**B**) to obtain heatmaps of the gene expression. The genes within 70% percentile of differential expression were then selected and plotted (**C**). Error bars: SEM, *n* = 4. * *p*-value < 0.05, 2-way t-test, Holm-Sidak method.

Figure 6. Mathematical Modeling of the Contribution of Individual Currents and Calcium Handling Machinery to the Action Potential of Monolayers and MPS. A) Schematic of the model. **B)** Examples of experimentally measured individual currents (data obtained with BeRST-1) used as model inputs. **C)** Representative simulated currents based on the corresponding color of experimentally measured current. **D-G)** Simulated current fluxes. **D)** Major potassium currents (I_{K1} and I_{Kr}, hERG). **E)** Na^+ current. **F)** Sodium-calcium exchange current. **G)** *L*-type calcium current. **H-J)** Simulated calcium dynamics. **H)** Ryanodine-receptor flux. **I)** SERCA pump activity. **J)** Intracellular Ca^{2+} diffusion. **K)** Surface/volume ratio of cardiomyocytes predicted from simulations. Media type and culture type (MPS vs. 2D Monolayer) had global effects (1-way ANOVA) in panels F and J. * $p < 0.05$, ** $p < 0.01$, *2*-way *t*-test.

Figure 7. Kinetic Parameters of Calcium and Potassium Currents obtained from Mathematical Modeling. A) Dynamics of simulated I_{Na}, I_{NaCa}, I_{CaL}, I_{K1} and I_{Kr} for one representative sample from each treatment group. **B-E)** Integrated current flux in the time-frame starting 100msec and ending 200msec after the peak in action potential simulated for each treatment group. **B-C)** Calcium current fluxes (B)

I_{NaCa} and (C) I_{CaL}. **D-E)** Potassium current fluxes (D) I_{Kr} and (E) I_{K1}. ** $p < 0.01$, 2-way *t*-test. The sample in A) was chosen as the sample with the median value for integrated I_{NaCa} current density in B.

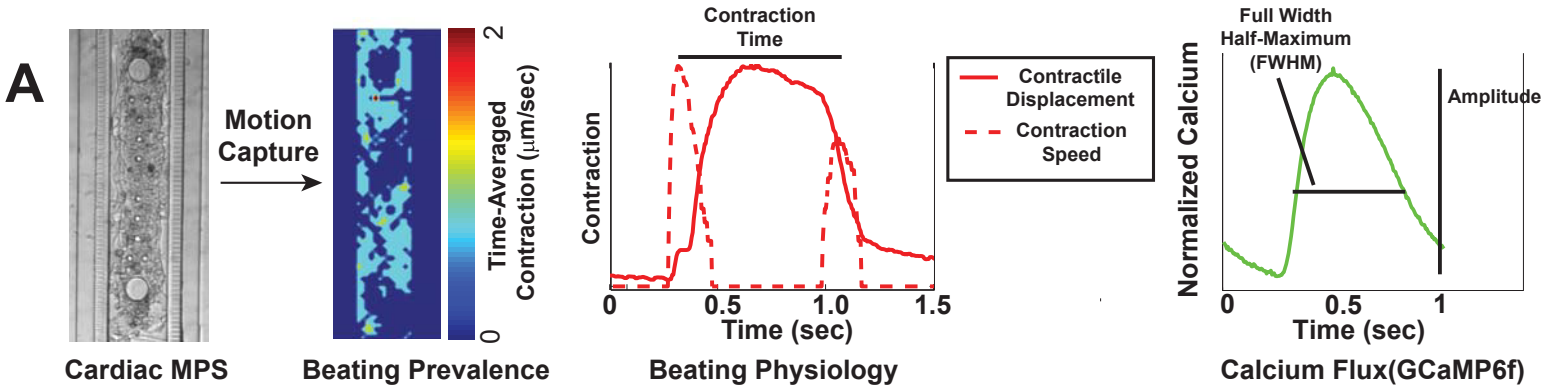

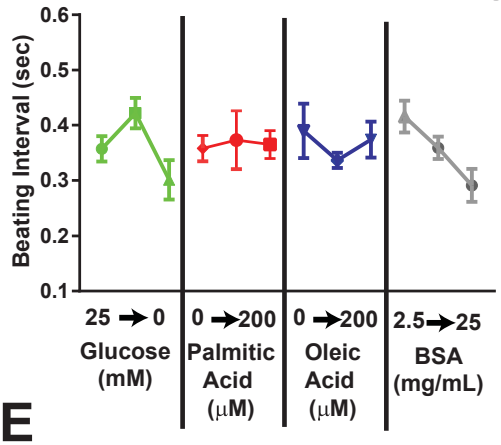

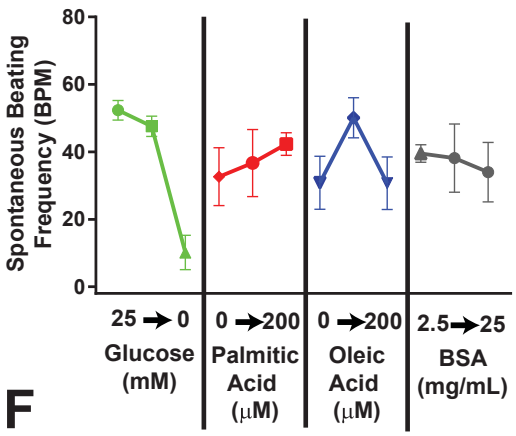

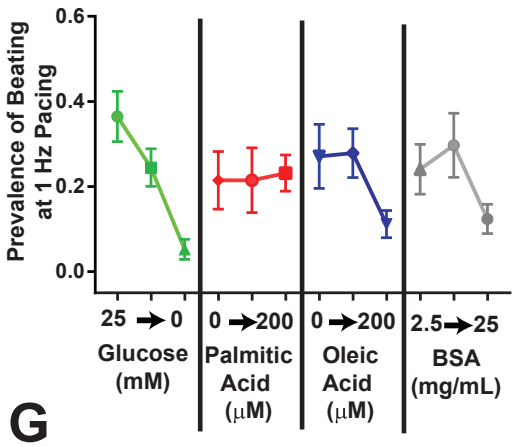

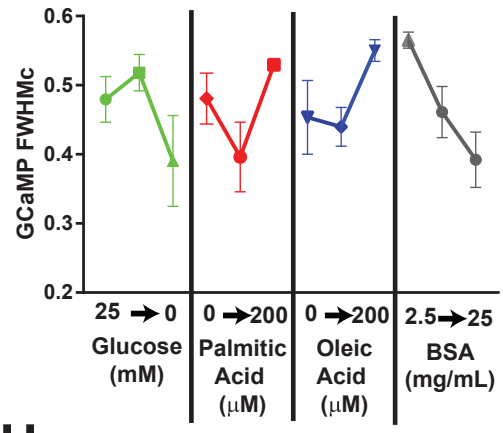

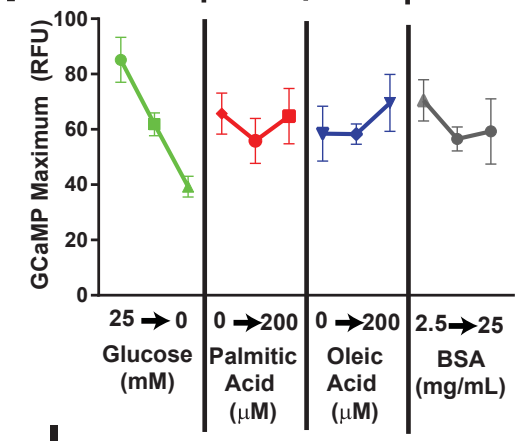

G

	Glucose	Palmitate	Oleate	BSA
Beating Interval	*			*
Spontaneous BPM	**			
Prevalence	**			
GCaMP Maximum	**			
GCaMP FWHMc				**

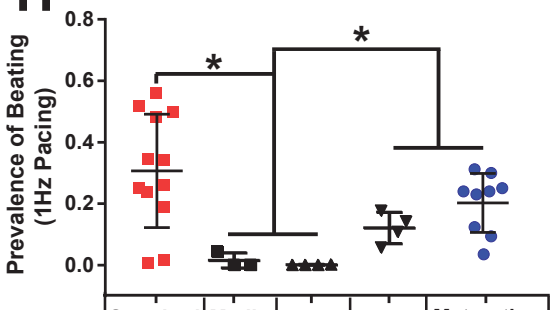

	Standard Media	Media 7	Media 8	Media 9	Maturation Media
Glucose (mM)	25	0	0	0	2.75
Oleate (μM)	0	200	0	100	200
Palmitate (μM)	0	0	100	200	100

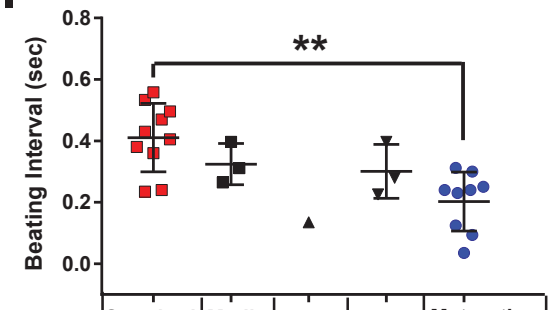

	Standard Media	Media 7	Media 8	Media 9	Maturation Media
Glucose (mM)	25	0	0	0	2.75
Oleate (μM)	0	200	0	100	200
Palmitate (μM)	0	0	100	200	100

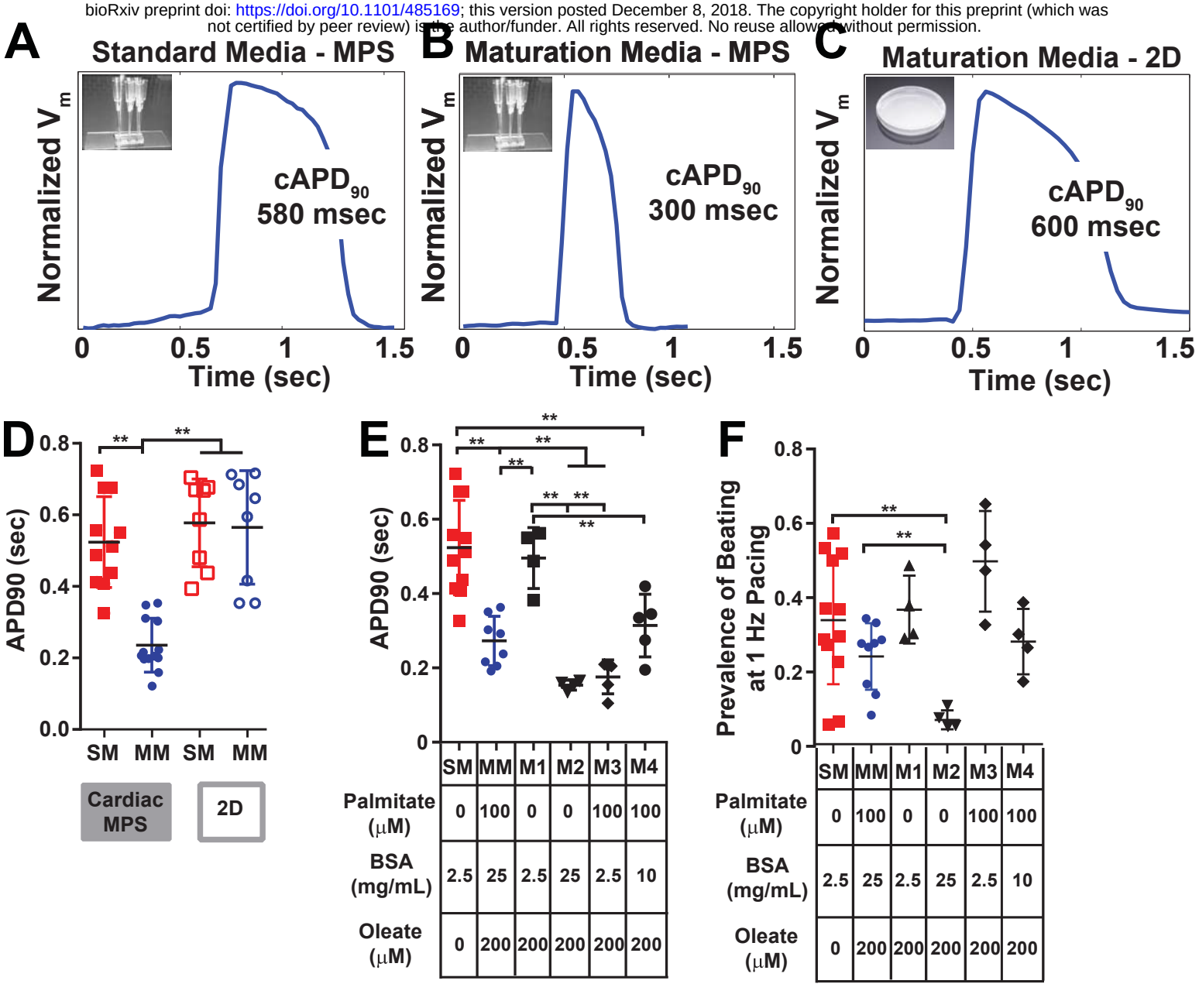

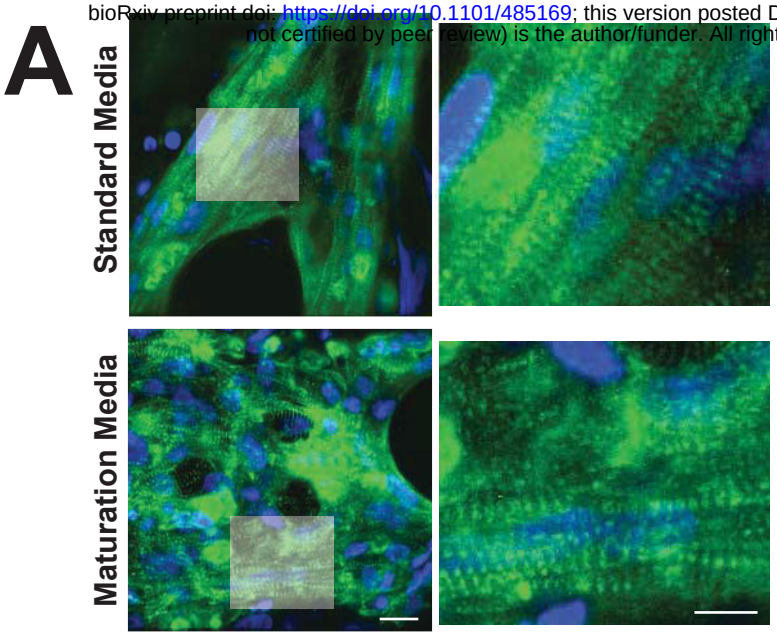

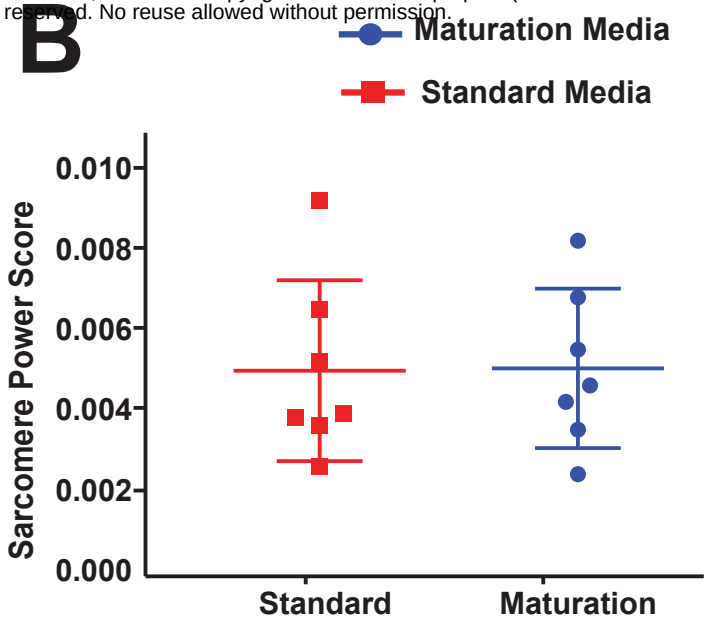

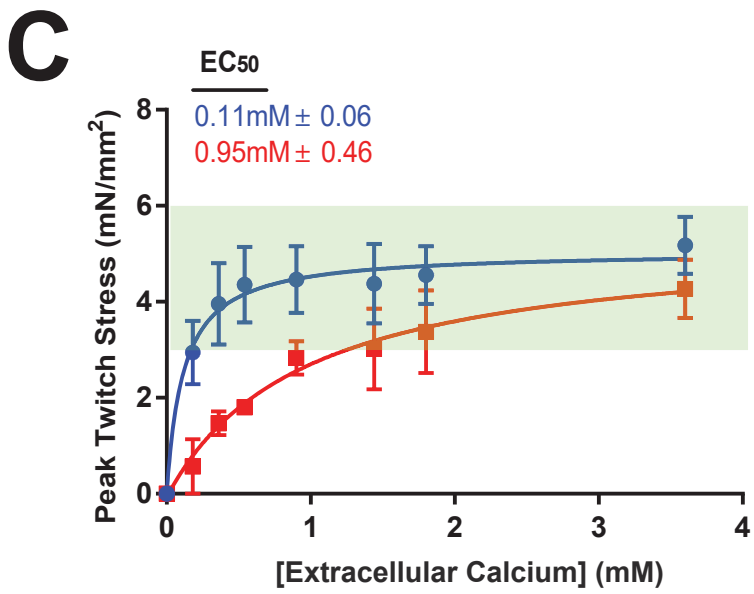

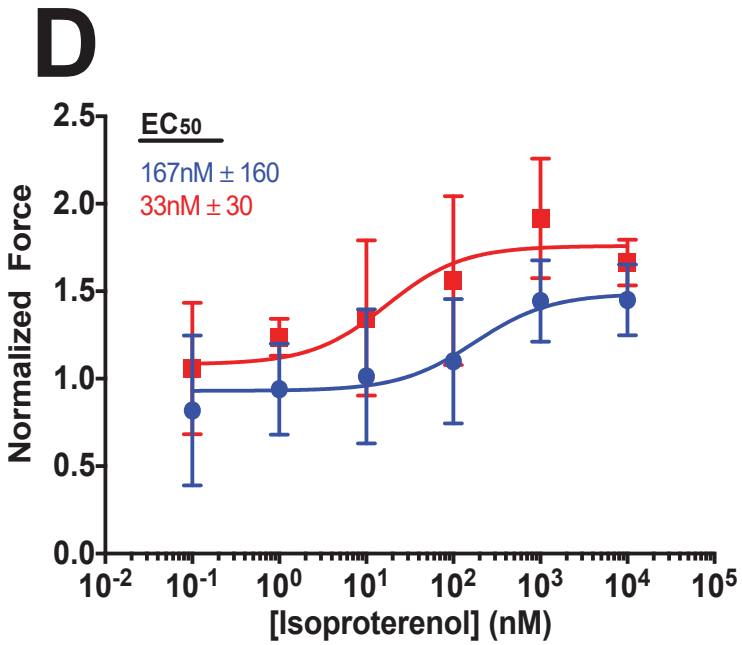

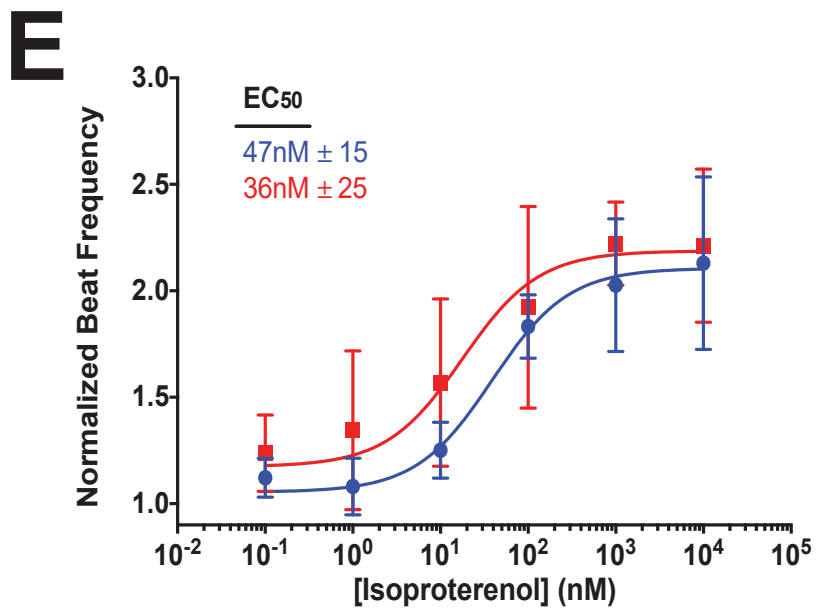

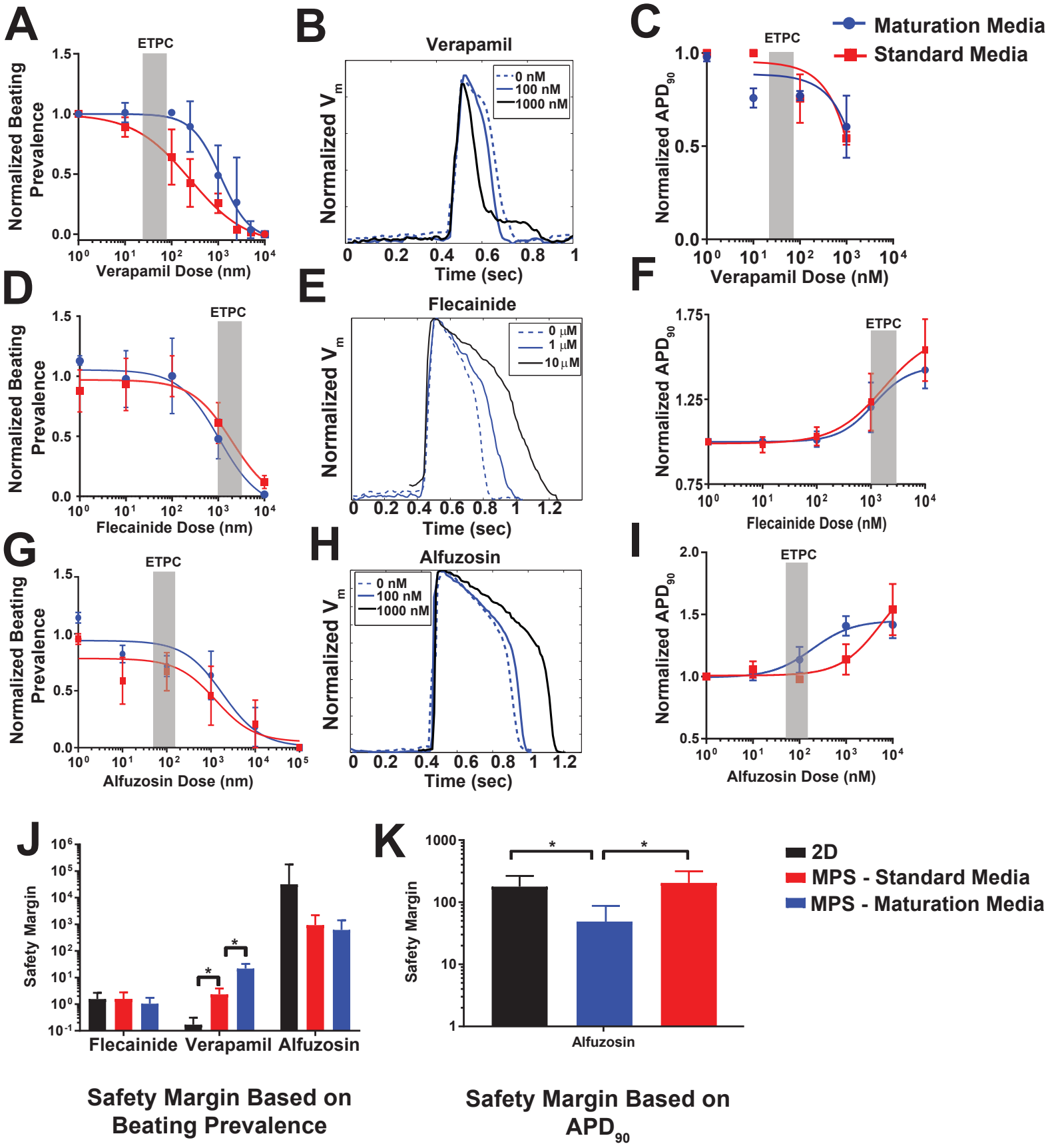

Safety Margin Based on Beating Prevalence

Safety Margin Based on APD_{90}